

Laser Audio Communication System

Nicolas Tanaka, Jan Strzeszynski, Soojung Bae

MIT Analog Electronics Laboratory 6.2040

Spring 2024

Abstract

While radio frequencies (RF) are widely used for long-range communication, laser communication is envisioned as an alternative for inter-orbit linkages, allowing point-to-point wireless transmission with higher efficiency and bandwidth. In this paper, we present a laser communication system that allows wireless transmission of an audio signal using a Frequency Modulated (FM) laser emission. Based on the input audio signal from a microphone, we frequency-modulate the laser driver using a voltage-controlled oscillator. On the receiving side, a phase-locked loop demodulates the laser signal received by a photodiode, reproducing the audio signal through an external speaker. This project is completed entirely in the analog domain, using inexpensive discrete circuit components for the fully functioning system.

1. Introduction

Laser communication is an effective method of wireless communication, especially in outer space and satellite systems. It is particularly useful in these systems because of its high power efficiency over long distances. While a radio signal is broadcasted in all directions, the laser beam is collimated—all the energy is concentrated in one direction and thus can reach much further before it is completely attenuated. This leads to yet another reason why laser communication might be preferred over radio, which is information security. When information is transmitted over radio it is available to be picked up by anyone within range. For a laser, on the other hand, the signal needs to be physically intercepted to receive the information. This also means that laser communication avoids creating unnecessary RF noise in the surrounding space, which could interfere with other RF signals.

In our project, the laser signal is going to be frequency modulated. This approach was chosen because of its high resiliency to noise (compared to amplitude modulation) which is especially important when transmitting over long distances like the laser is capable of.

1.1 System Overview

As shown in Figure 1, our system consists of opto-isolated transmitter and receiver modules communicating from a laser to a photodiode. We use frequency modulation for encoding the audio input into a laser signal. This provides sufficient noise tolerance for communication even under uncontrollable optical settings such as noise from ambient light. On the transmitting end, an audio signal from the microphone is amplified to match the optimal operating range of the Voltage-Controlled Oscillator (VCO). The amplified signal then drives the VCO, modulating the output signal by linearly converting the voltage level into the 490-520 kHz frequency domain. Finally, the modulated signal drives the laser to transmit the encoded data. On the receiving end, the photodiode, in alignment with the laser, converts the laser amplitude into a current. We use a transimpedance amplifier to change this to a voltage signal which will drive the Phase-Locked Loop (PLL). The PLL demodulates the FM signal to audio by detecting the input frequency and inverting it to the corresponding voltage level. Finally, the output audio is reproduced by driving an external speaker.

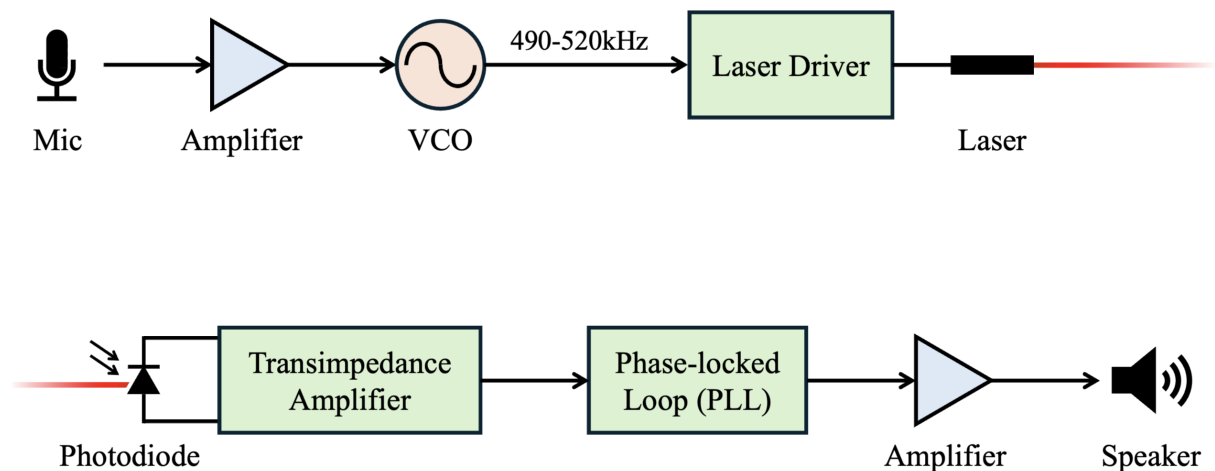


Figure 1: **System overview.** Our system consists of four main parts: Audio, Modulation, Demodulation, and Optical path.

2. Optical Path

[Nicolas Tanaka]

The purpose of the optical path is to transmit and receive a sinusoidal voltage signal around 500 kHz using a laser. The input to this system is expected to be a 450 - 550 kHz sinusoidal voltage signal, with amplitude 200 mVpp - 4 Vpp and no DC offset. These values depend on the behavior of the Colpitts oscillator, and the circuit can be easily modified once the Colpitts oscillator output is determined.

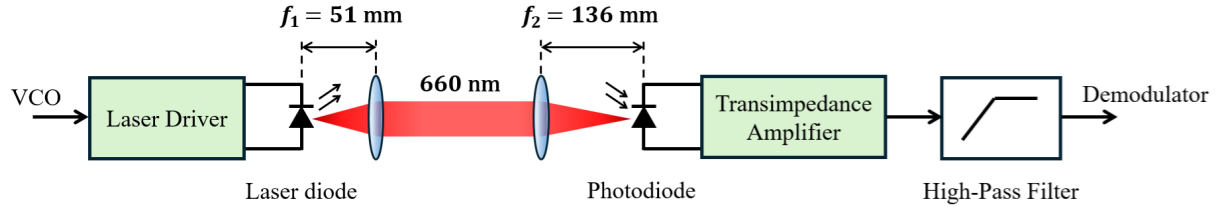


Figure 2: **Laser Subsystem.** The laser subsystem consists of a laser driver, optical path, transimpedance amplifier, and high-pass filter. Two lenses are used to collimate the laser beam.

2.1 Laser Driver

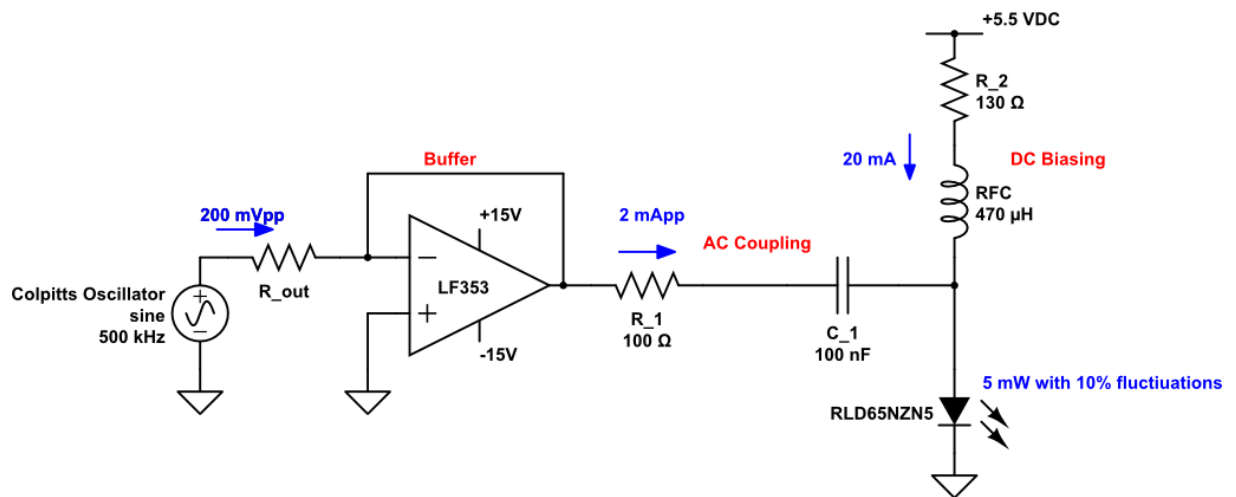


Figure 3: **Laser Driver Circuit.** Laser driver receives a 500 kHz sine wave from the Colpitts Oscillator and produces a 5 mW laser output with 10% fluctuations. The circuit consists of an AC signal path and a DC biasing circuit.

The laser driver circuit is shown in Figure 3. The output of the Colpitts oscillator is expected to be a 450-550 kHz sine wave, with amplitude 200 mVpp - 4 Vpp and no DC offset. The output resistance of the oscillator system is reasonably large, thus the output of the oscillator is treated as an AC voltage source with source resistance R_{out} . To deal with this problematic source resistance, this signal is first buffered using an LF353 operational amplifier. Since the output resistance of the buffer is approximately zero, the buffered signal can be treated as an ideal AC voltage source.

2.1.1 DC Biasing

According to the RLD65ZNZ5 laser diode datasheet (Semiconductor, 2019), the laser diode has a turn-on voltage $V_{on} \approx 2.2V$. To DC bias the laser diode, a voltage supply and resistor can be used as shown on the right side of Figure 3. When the voltage supply is at 5.5V, the resistor voltage becomes $V_{DD} - V_{on} \approx 3.3V$. Thus the resistor acts as a

current source providing around 20-30mA of current. This current is translated into a laser output power of 5mW.

To decouple the AC signal from the DC biasing, we use a Radio Frequency Choke which becomes short at DC but has high impedance at AC. In addition, we use a coupling capacitor C1 to modulate the laser output with an AC input signal.

2.1.2 AC Modulation

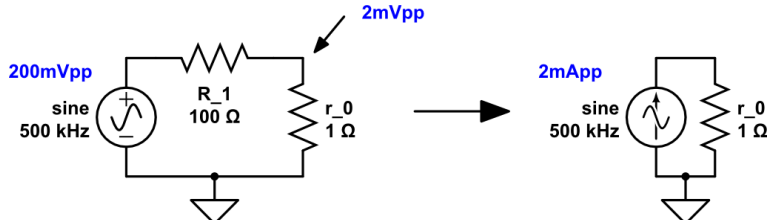


Figure 4: **Laser Driver Small Signal Model.** Left: Input voltage source drives a resistor divider where r_o is the output resistance of the diode. Right: The voltage source and R_1 act as an AC current source with 2mApp.

The small signal equivalent circuit is shown in Figure 4. The buffered output of LF353 op-amp acts as an ideal voltage source. The coupling capacitor C1 has 3Ω impedance at 500 kHz, negligible to R1. The laser diode obeys the diode current-voltage relationship, and thus its small signal behavior can be characterized as:

$$I_D + i_d \approx I_0 e^{V_D/V_T} \cdot e^{v_d/V_T} \approx I_D + \frac{I_D}{V_T} \cdot v_d + \mathcal{O}\left(\left(\frac{v_d}{V_T}\right)^2\right). \quad (1)$$

And thus for $v_d \ll V_T = 26\text{mV}$, the small signal resistance of the diode can be modeled as:

$$r_o = \frac{\partial V_D}{\partial I_D} = \frac{V_T}{I_D} \approx 1\Omega. \quad (2)$$

Small v_d is achieved by choosing the large R1 value. This ensures the diode acts within a linear current region, minimizing the undesired distortion or harmonics of 500kHz. Furthermore, the voltage supply and R1 act as a current source with 2mApp, directly translating current into output light.

2.2 Photodiode and Transimpedance Amplifier

To receive the laser light, we chose to use a PDB-C142 photodiode (Optoelectronics, 2016) which has 0.3 [mA/mW] light response at 660nm wavelength. Since we are expecting to receive 3mW of laser light, the photodiode produces $\approx 1\text{mA}$ of DC current. To turn this current into a voltage signal, a transimpedance amplifier is used which creates an output voltage $V = -I \cdot R_1 \approx -3\text{V}$ DC. This ensures the transimpedance amplifier has an optimal signal-to-noise ratio while not saturating the LF353 op-amp. Optimum C1 value is derived from the following equation (Hashemi, 2015):

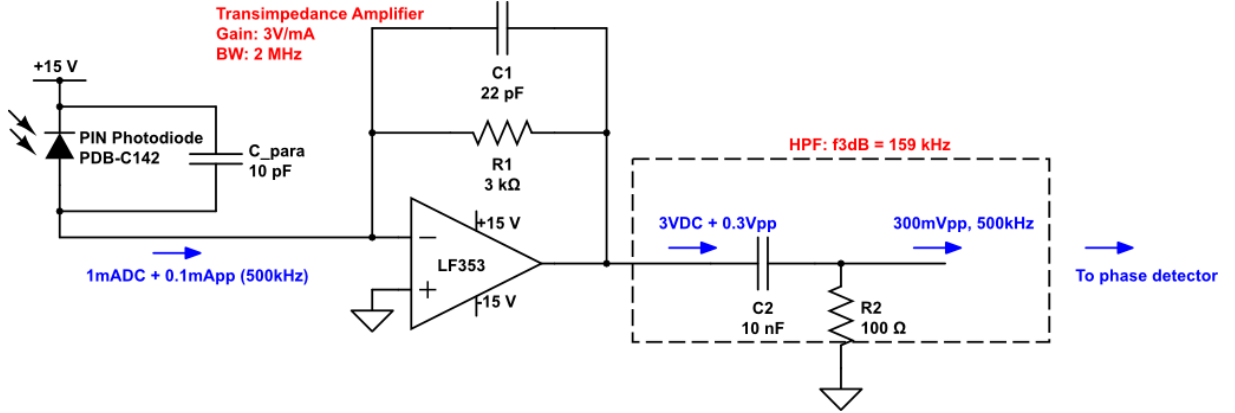


Figure 5: **Laser Receiver Circuit.** The photodiode produces a current proportional to the laser amplitude light it receives. This current is converted into a voltage through a transimpedance amplifier, which is then high-pass filtered to remove the 3V DC offset.

$$C_{opt} = \sqrt{\frac{C_{IN}}{2\pi(GBWP)R_F}}, \quad (3)$$

where $C_{IN} = C_{diode} + C_{para} \approx 20\text{pF}$, and Gain Bandwidth Product (GBWP) is 3MHz. The bandwidth of the transimpedance amplifier is given by:

$$f_{-3dB} = \sqrt{\frac{GBWP}{2\pi R_1 C_1}}. \quad (4)$$

which theoretically should be $\approx 2\text{MHz}$, but in practice measured as 700kHz due to the limited op-amp slew rate of 13V/μs. To remove the DC offset and low-frequency environmental noises, we put a high-pass filter with $f_{-3dB} = 159\text{kHz}$.

2.2.1 Photodiode and TIA Performance

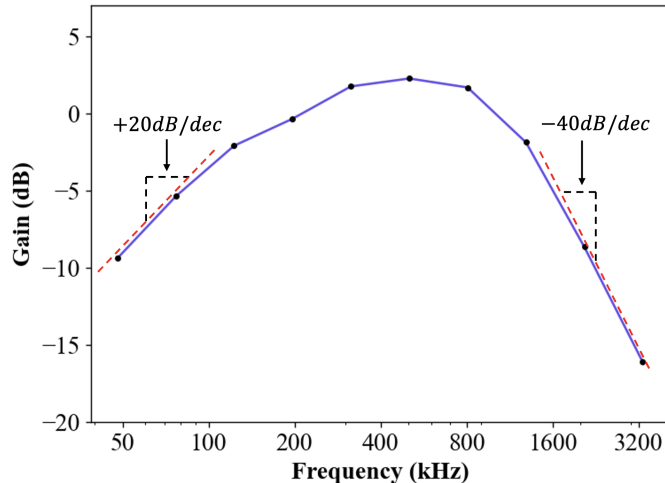


Figure 6: **Transimpedance Amplifier Gain vs. Frequency.** The band-pass filter is formed by 20dB/dec at low-frequency (from the high-pass filter) and -40dB/dec at high-frequency (from the transimpedance amplifier and the LF353's slew rate).

To test our TIA, the output of the LF353 op-amp and the high-pass filter were measured. The laser diode was driven with 20mA DC current and 2mApp sinusoid at 500kHz, producing the 5mW laser power with a 10% power fluctuation. To verify the TIA functionality, we expect DC voltage with 10% AC fluctuations as well.

Figure 6 shows the measured overall gain of the optical system. This system was optimized to have the highest gain around 450 - 550 kHz.

3. Audio

[Jan Strzeszynski]

The audio subsystem is divided into two parts at the two ends of the signal chain. It allows the user to both interact with the circuit (through the microphone) and receive its output (through the speaker). Both the microphone and the speaker require amplification circuits to output a signal with desired parameters.

3.1 Microphone

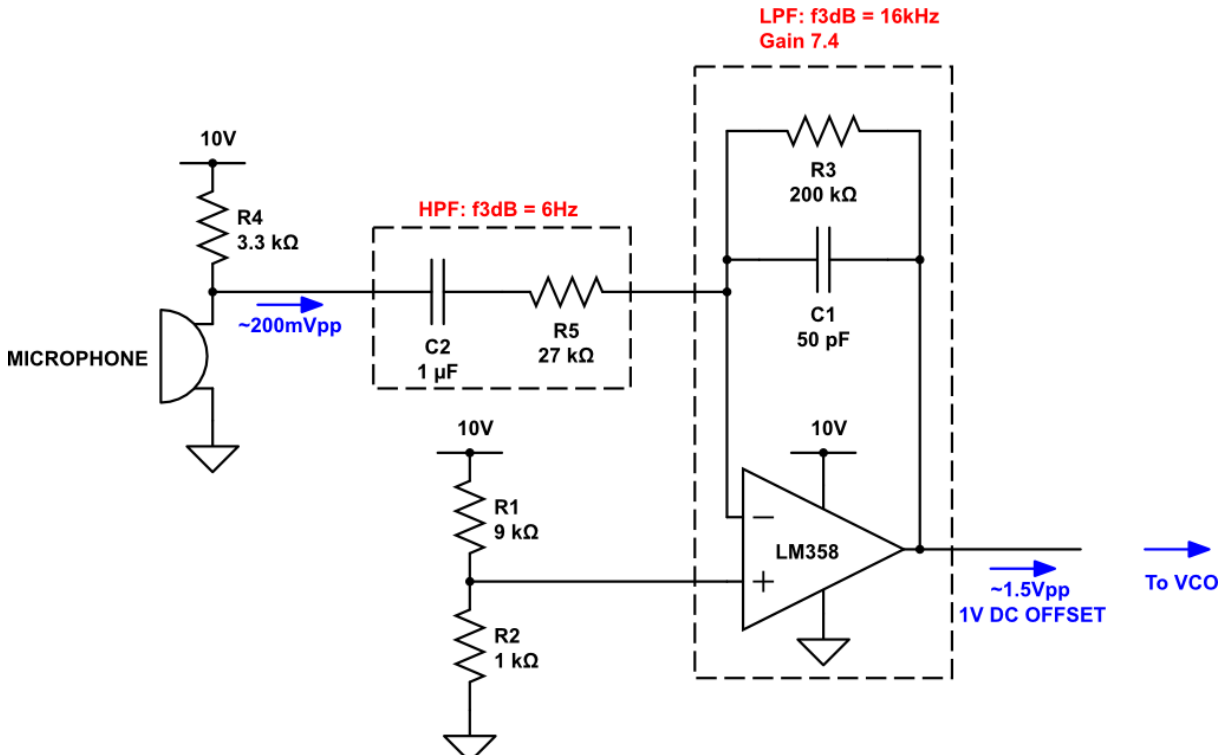


Figure 7: **Microphone amplifier.** The amplifier implements a band-pass filter between 6Hz-16kHz and has a gain of 7.4 to produce an output of 1.5Vpp with 1V DC bias

The microphone amplifier circuit is depicted in Figure 7. The microphone amplifier takes in around 200mVpp signal from the microphone (this is an approximate value for normal speech) and amplifies it to a 1.5Vpp signal with 1V DC offset which is then used by the VCO. Additionally, the amplifier acts as a band-pass filter. The low-pass filters out

any noise that the microphone might pick up above 16kHz and the high-pass removes the DC offset from the output of the microphone. The cutoff frequencies for this band-pass (6Hz-16kHz) are chosen such that they still allow through most of the hearing range of frequencies.

3.2 Speaker Driver

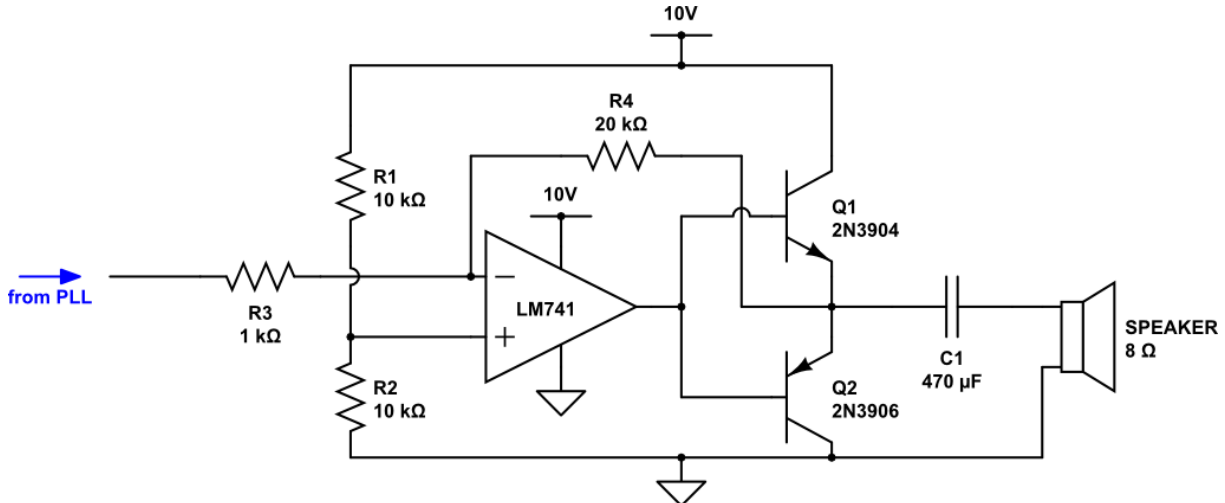


Figure 8: **Speaker amplifier.** An amplifier with a gain of 20 and a push-pull stage at the output which minimizes the output impedance to drive the 8Ω speaker.

The speaker driver circuit is depicted in Figure 8. The speaker driver takes in a demodulated audio signal from the PLL and amplifies it with a gain of 20 in order to make it audible when played through the speaker. The circuit uses a push-pull stage at the output because the 8Ω speaker requires low impedance at its input. Additionally, the signal is passed through a large capacitor right before the speaker in order to eliminate the DC offset of the signal.

4. Modulation

[Soojung Bae, Jan Strzeszynski]

On the transmitting side, the amplified audio signal needs to be modulated before being transmitted by the laser. This is achieved using a Colpitts Voltage-Controlled Oscillator, described below.

4.1 Voltage-Controlled Oscillator (VCO)

As shown in Figure 9, we use a Colpitts voltage-controlled oscillator to encode the input audio signal into FM modulated sinusoidal wave. A Colpitts oscillator generates output with resonating frequency by forming a feedback loop within its LC tank (Colpitts, 1918). Particularly, viewing D1 and D2 as an equivalent capacitor C_2 at an operating frequency,

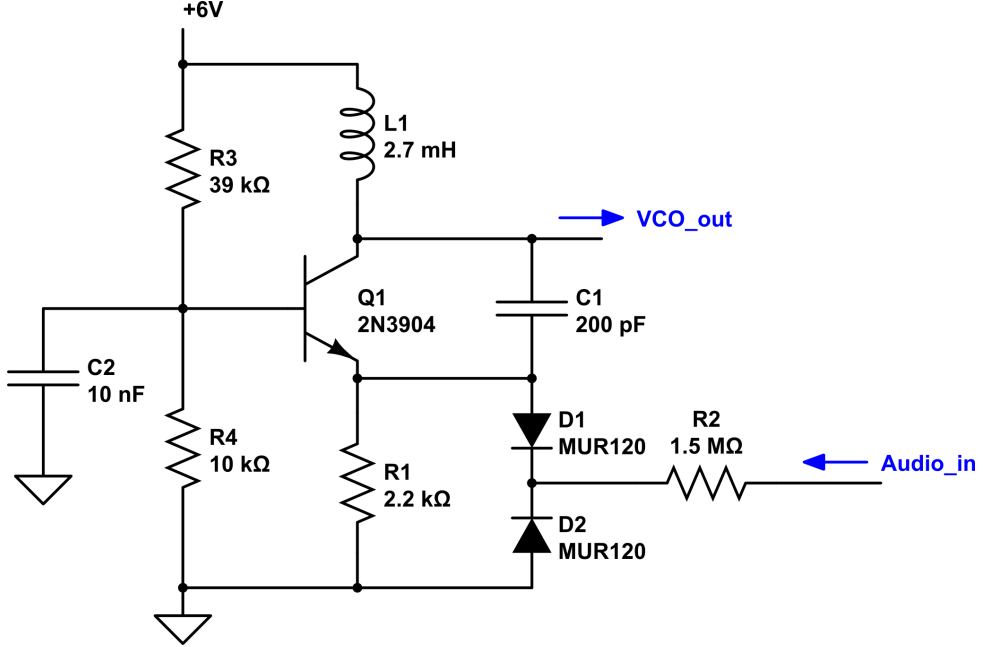


Figure 9: Hagen Colpitts Voltage-Controlled Oscillator.

Q1's emitter receives voltage divided result of the collector between C1 and diode capacitors. This non-inverting feedback input is amplified with a common base configuration of Q1, driving the LC resonance. Therefore, the total loop gain is determined by the voltage dividing ratio and emitter gain, where for the ideal oscillation the loop gain should be 1. The resonant frequency of a Colpitts oscillator is derived from a small-signal model of transistors. Assuming L1 (RFC) has a series resistance value of r and Q1 with r_π from the Hybrid- π model, the resonant frequency is approximated as (Stave, 2019):

$$\omega^2 = \frac{1}{L_1} \left(\frac{1}{C_1} + \frac{1}{C_2} + \frac{r}{r_\pi C_2} \right). \quad (5)$$

In addition to enabling the oscillation, the output frequency should be adjustable using our signal input. We use a varactor diode with varying capacitance values dependent on the reverse bias voltage. Varactor diodes form a thickness-varying depletion region depending on a DC reverse bias voltage. Thus at high frequency, diodes act as variable capacitors, while rejecting the DC current passing through.

Accordingly, we can interpret the diodes in Figure 9 with DC and AC equivalent components. In DC, D1 and D2 diodes conduct no current through as they are reverse biased. Therefore, audio input directly biases the diodes regardless of the R_2 value. In AC, on the other hand, the diodes act as series capacitors with R_2 connected to an external circuit. However, the capacitors are effectively isolated from the external circuit as R_2 has a high resistance value. Hence DC biasing and AC characteristics are decoupled from each other, simplifying the analysis of VCO properties.

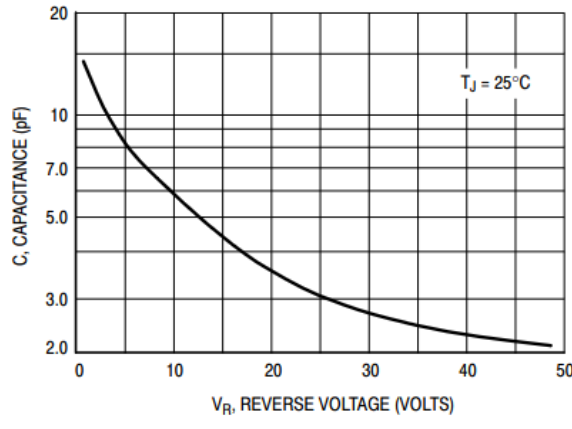


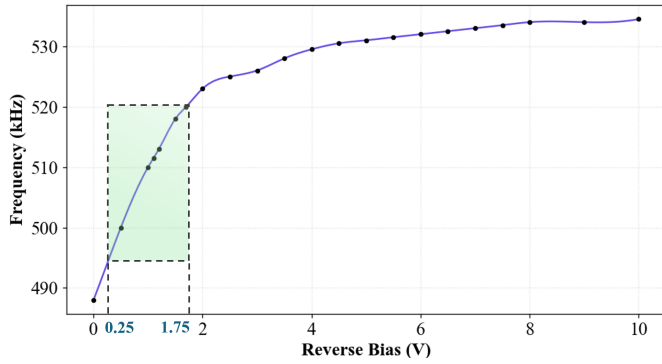
Figure 10. Typical Capacitance

Figure 10: Capacitance vs. Reverse Voltage of MUR120 (Onsemi, 2013). Substantial variance in capacitance over voltage is necessary to construct a VCO with adequate frequency to voltage response

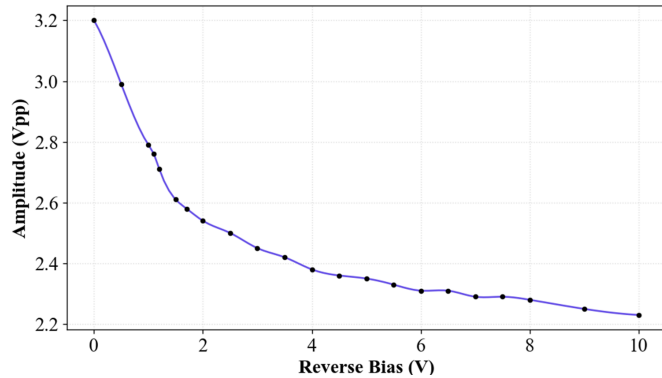
4.1.1 VCO Performance

The relation between the reverse voltage and capacitance for the varactor diodes used in the VCO is established on Figure 10. The exact capacitance to reverse voltage function for diodes in the VCO is difficult to model due to the presence of two diodes with common cathode as well as one of the anodes not being grounded. Regardless, the response of the isolated varactor diode might suggest a correct behavior when inside the system, which has then been verified by measuring the response of the complete VCO.

The frequency and amplitude data collected for the VCO for a range of reverse bias voltages is shown in Figure 11. As established in Section 3, the signal passed to the VCO from the microphone amplifier is a 1.5Vpp signal with 1V DC offset. These signal parameters were chosen to operate the VCO in its optimal range. The operation range of the VCO is marked by the green area in Figure 11a. In this area, the frequency-to-voltage response is nearly linear (which helps with the stability of the PLL) and is also relatively steep which makes the system more resistant to noise.



(a) Frequency vs Reverse bias



(b) Amplitude vs Reverse bias

Figure 11: **VCO Measurements.** The green rectangle is the operating region of the VCO. The response in this region is nearly linear and relatively steep, which are the optimal conditions for the VCO.

5. Demodulation

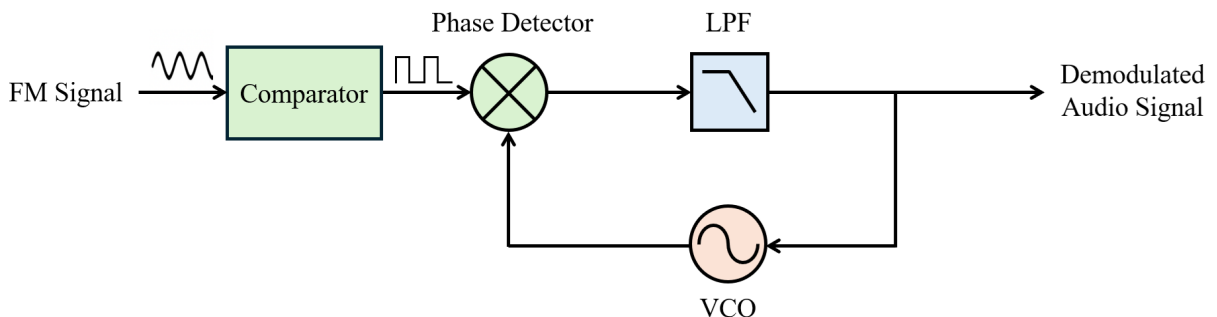


Figure 12: **Demodulator Subsystem.** The frequency modulated signal is passed through a comparator to turn it into a square wave. The Phase-Locked Loop demodulates the signal, reproducing the original audio signal.

[Nicolas Tanaka]

One technique commonly used to demodulate a frequency-modulated (FM) voltage signal is a phase-locked loop. Figure 12 illustrates the negative feedback loop. The first stage of the feedback loop is a phase detector and low-pass filter (LPF). The phase detector is commonly built using an exclusive-or gate (XOR), which outputs a phase

difference between input signals. The low-pass filter is needed to extract the DC phase error. The phase difference is fed into a Voltage-Controlled Oscillator, whose output is fed back into the phase detector. This negative feedback loop locks the phase difference between the VCO and FM input to a constant value, thereby driving the VCO to match the FM signal's frequency. Thus, the input to the VCO is the demodulated FM signal, which is the original audio signal.

5.1 Comparator

[Soojung Bae]

Since the Phase Detector requires a digital input signal, we need to convert the sinusoidal signal received from the laser to a square wave. We use a Schmitt Trigger to robustly detect input signal edges. A preamplifier is used in the preceding stage to set the signal bias and amplitude appropriate for the Schmitt Trigger.

5.1.1 Preamplifier

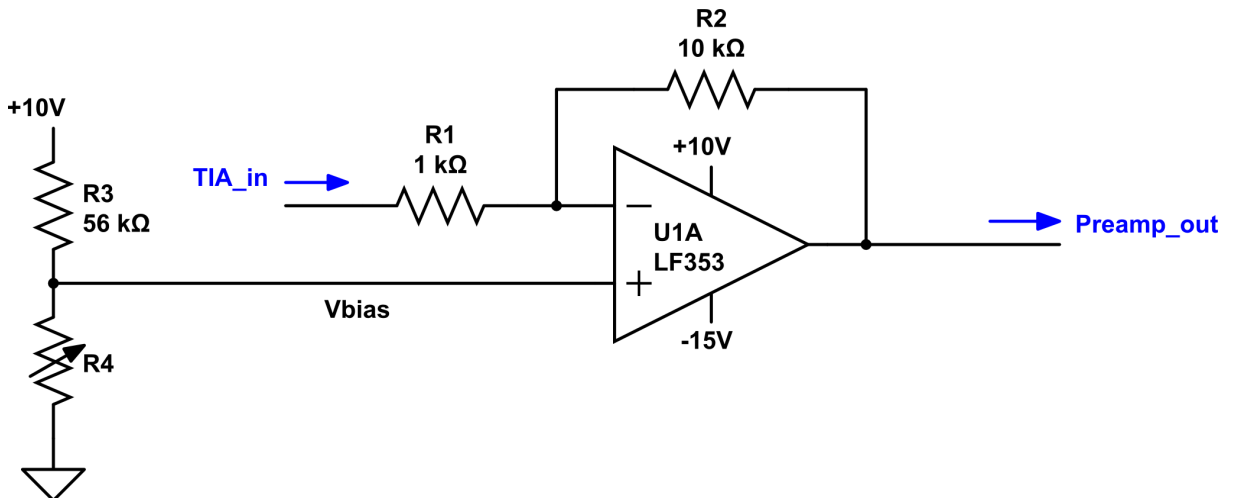


Figure 13: **Preamplifier Circuit**. Divided into an adjustable voltage divider for biasing (left) and an inverting amplifier with $A = -10$ (right).

We use preamplifier stage to satisfy the input specification of our Schmitt Trigger—minimum of $1V_{pp}$ and 1–2V DC bias. As shown in Figure 13, preamplifier consists of an inverting amplifier with an adjustable bias. Assuming 500kHz input signal v_{in} , the circuit output is:

$$v_{out} = v_{in} \cdot \frac{R_2}{R_1} + V_{dd} \cdot \left(\frac{R_3}{R_3 + R_4} \right) \cdot \left(1 + \frac{R_2}{R_1} \right). \quad (6)$$

With a gain of 10, 300mVpp AC input achieves a sufficient amplitude of 3Vpp to trigger the comparator threshold.

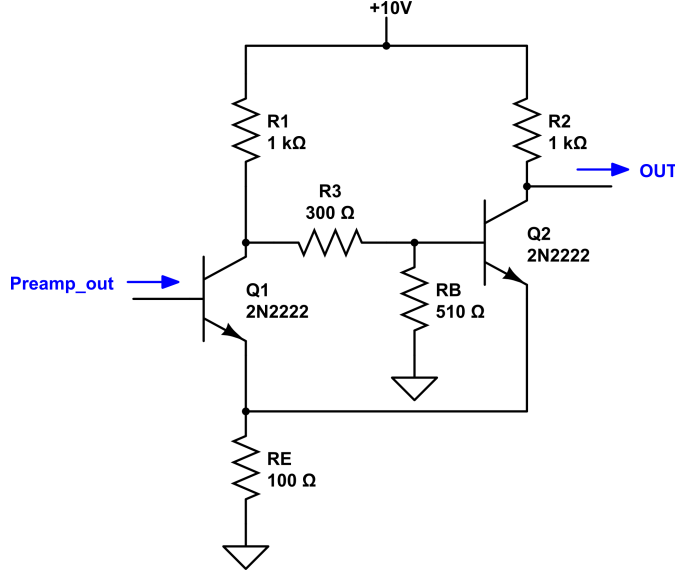


Figure 14: BJT Schmitt Trigger Circuit.

5.1.2 Schmitt Trigger

Schmitt Trigger can be used as a comparator with a hysteresis characteristic that can robustly detect transition edges by rejecting certain noise levels. While a comparator can be simply implemented with operational amplifiers, our system requires near-ideal square wave operating at 500kHz with $10V_{pp}$, which results in $> 300V/\mu s$ to account for sharp rising and falling edges. However, most of inexpensive op-amps have limited slew rate or gain bandwidth; for example, LF353 wide-bandwidth op-amp has $13V/\mu s$ of slew rate (Instruments, 2016). Therefore, as shown in Figure 14, we implemented our system with bipolar junction transistors (BJTs), which have fast switching speed and high gain.

The circuit's operation consists of two distinguished states. In the first state, input is low, and Q1 stays off ($V_{BE,Q_1} < V_{BE} \approx 0.7V$). This turns Q2 on, which pulls down the output to V_{OL} by the current through R2. On the other hand, the transition happens when $V_{IN} > V_+$, turning Q1 on pulling down the base voltage of Q2. The output is V_{DD} here since Q2 inactivates. The circuit transitions back to the first state for $V_{IN} < V_-$ when Q1 turns off again.

Assuming constant turn-on voltage $V_{BE} \approx 0.7V$ and current gain $\beta_F \approx 150$, the turn on voltage is determined by:

$$\frac{V_{DD} - V_+}{R_1 + R_3} = \frac{V_+}{R_B} + \frac{1}{1 + \beta_F} \frac{V_+ - V_{BE}}{R_E} \Rightarrow \therefore V_+ \approx 2.77V. \quad (7)$$

The condition for determining V_- is when $V_{CE,Q1} < V_{CE,sat}$ ($0.3V < V_{CE,sat} < 1.0V$ for 2N2222), therefore:

$$\left(\frac{V_{DD}}{R_1} - \frac{\beta_F}{\beta_F + 1} \frac{V_- - V_{BE}}{R_E} \right) \cdot \left(\frac{1}{R_1} + \frac{1}{R_3 + R_B} \right)^{-1} \cdot \frac{R_B}{R_3 + R_B} - V_{BE} < V_- - V_{BE} + V_{CE,sat} \quad (8)$$

$$\therefore 0.99V < V_- < 1.17V. \quad (9)$$

5.1.3 Schmitt Trigger Performance

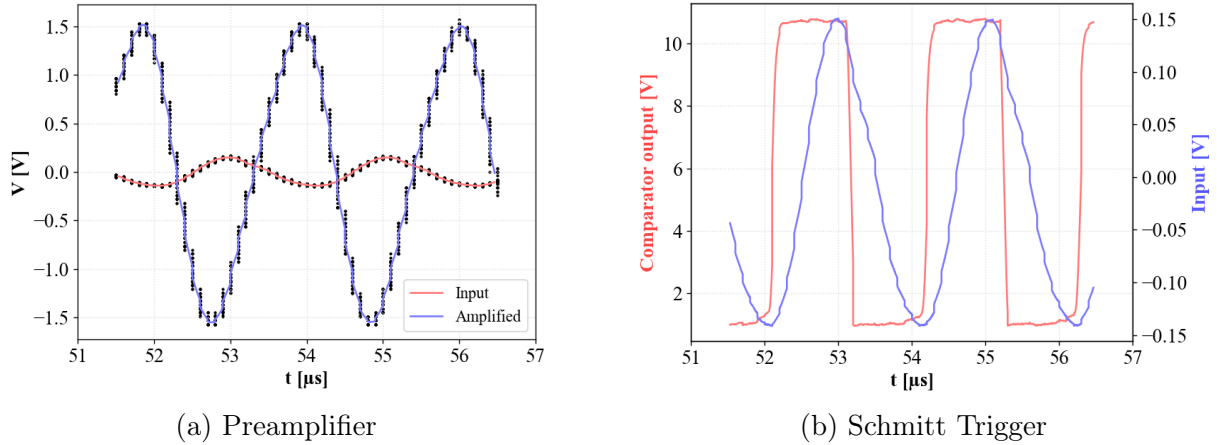


Figure 15: **Comparator Measurements.** The preamplifier input and output (left) and the schmitt trigger result converting sinusoidal input to a square wave (right).

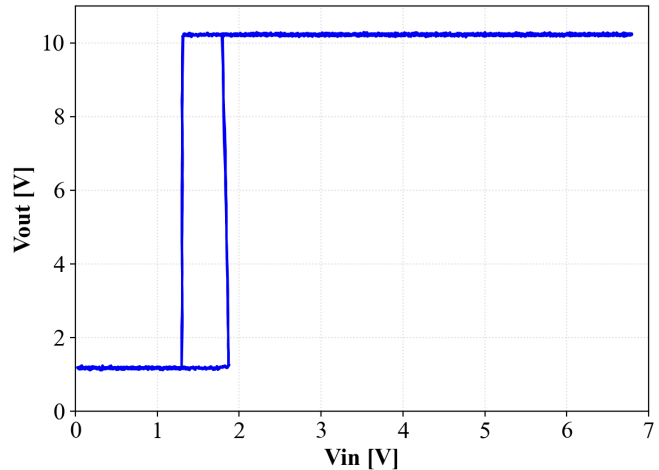


Figure 16: **Hysteresis of Schmitt Trigger.** The state transition follows a counter-clockwise path on the graph.

As shown in Figure 15a, the preamplifier has a gain of 10.3, amplifying the 287 mV peak-to-peak input signal to 2.97 V_{pp} output. Since the LF353 operational amplifier is driven towards its bandwidth limit, we observe that there is a significant phase delay. However, phase delays would not affect the system's functionality since our demodulator can detect and lock into arbitrary phases.

Figure 15b shows the output of the Schmitt trigger with a preamplified signal as input. The circuit shows 50 ns rise time and 33 ns fall time (i.e., transition time between 30% and 70% of voltage difference). In addition, the Schmitt trigger had a hysteresis characteristic as shown in Figure 16. Specifically, state transitions occurred around $V_- = 1.20V$ and $V_+ = 1.87V$.

5.2 Phase-Locked Loop (CD4046)

[Nicolas Tanaka]

To accomplish frequency demodulation, the CD4046 phase-locked loop integrated circuit was used (Instruments, 2003). The pinout block diagram is shown in Figure 17. We operated the CD4046 IC at $V_{DD} = 10V$ and $V_{SS} = 0V$. The input signal to pin 14 is the FM signal, preferably a 0 - 10 V square wave. We used Phase Comparator I as the phase detector since it is an XOR gate. This signal is then low-pass filtered with $R_3 = 100k\Omega$ and $C_2 = 1 \text{ nF}$. The value of C_2 was experimentally tested to give locking up to a frequency modulation of 9 kHz. Next, this low-pass filtered phase error is fed into pin 9, the VCO input. The VCO oscillation frequency is determined by C_1 , R_1 , and R_2 . C_1 and R_1 are chosen to set the center frequency f_0 , which occurs when $VDD/2 = 5V$ is applied to VCO in. f_0 was set to be around 500kHz, by choosing $R_1 = 43k\Omega$ and $C_1 = 100\text{pF}$. The offset frequency f_{min} was set to be as large as possible to narrow the frequency range to 400 - 600 kHz. f_{min} is determined by R_2 , which was set to be $43k\Omega$ as well. The output of the VCO is connected to the second comparator input on pin 9, closing the feedback loop.

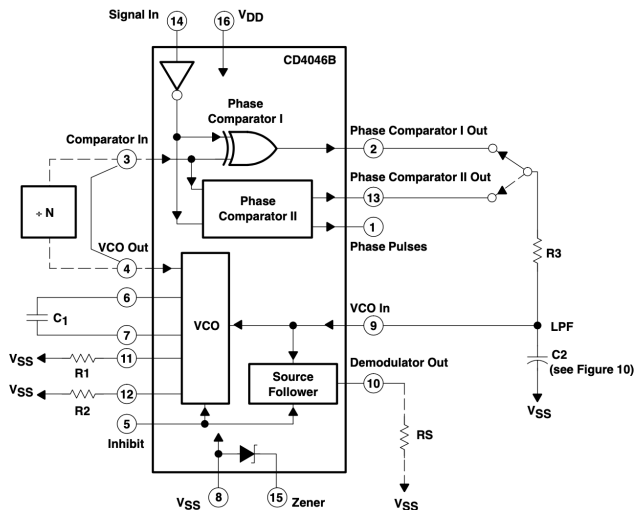


Figure 17: **CD4046 Phase-Locked Loop IC with external circuitry** (Morgan, 2003). R_3 and C_2 determine the cutoff frequency of the low-pass filter. R_1 , R_2 , and C_1 determine the frequency range of the VCO.

5.2.1 PLL (CD4046) Performance

First, the linearity and frequency range of the VCO were measured. The input to the VCO (pin 9) was swept from 0 VDC to 10 VDC, while the output of the VCO (pin 4) was measured on the oscilloscope. The frequency was recorded, and the result is shown in Figure 18. The slope of the transfer function is 30 kHz/V. This measurement demonstrates the VCO's high linearity, as well as frequency range from 400 - 600 kHz. This range is suitable for receiving the oscillations produced by the Colpitts oscillator.

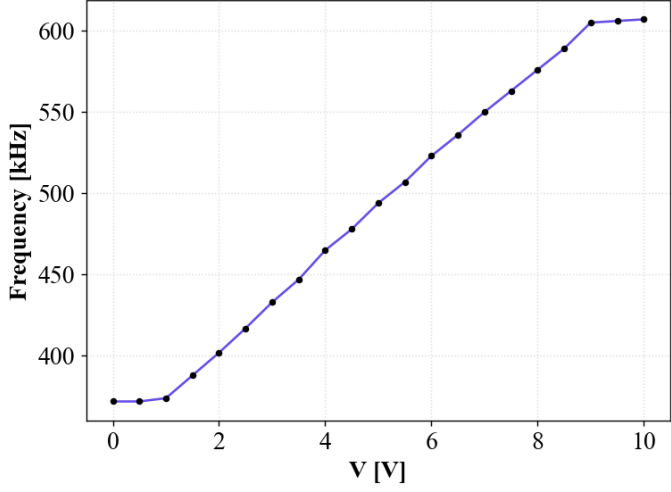


Figure 18: **Frequency vs. Input Voltage of CD4046's VCO.** The components connected to the CD4046 were chosen to center this curve around 500kHz with as narrow a range as possible.

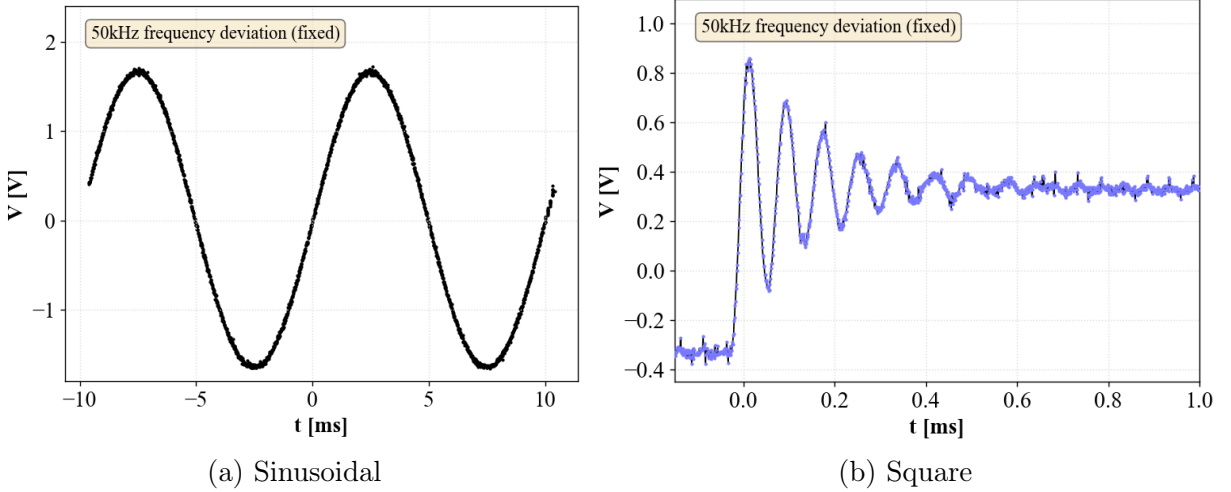


Figure 19: **PLL Demodulation Results.** Demodulated output signal from FM 100Hz sine input (left) and output ringing from step-function input (right). FM modulation with 50kHz frequency deviation is used for both graphs.

Secondly, we measured the CD4046 PLL's locking ability. With the function generator set to 0-10V square wave at center frequency 500 kHz, the frequency modulation setting was used. With the frequency deviation set to 50 kHz (100kHz peak to peak) and FM frequency set to 100 Hz, the output of the PLL (VCO in, pin 9), is expected to be a 100 Hz sine wave with amplitude $100\text{kHz} \left(\frac{1V}{30\text{kHz}}\right) = 3.3 \text{ Vpp}$. This was verified, as shown in Figure 19a.

Next, we measured the PLL's step response to examine the feedback stability. The result is shown in Figure 19b, which demonstrates a natural frequency of 12 kHz, and exponential decay time constant of $300 \mu\text{s}$. This demonstrates a pole in the feedback transfer function of around 12.5 kHz, at which point the feedback loop will become unstable.

Lastly, the PLL's frequency response was measured for various values of frequency deviation, as shown in Figure 24. The PLL sometimes went unstable and produced

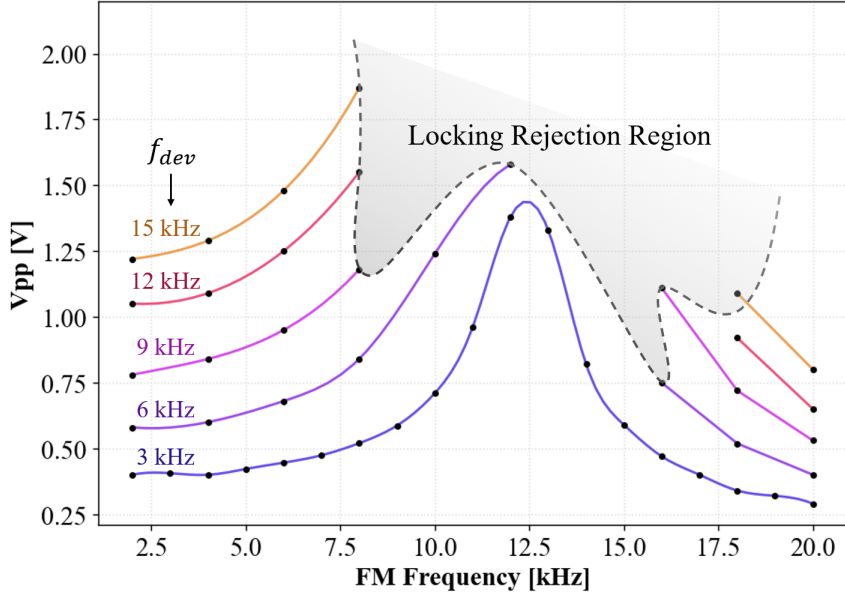


Figure 20: **Output Swing with FM Modulation Frequencies.** Locking Rejection Region denoted as a grey area, in which PLL fails to stabilize or produces undesired harmonics. Carrier frequency fixed to 500 kHz.

aperiodic or 500kHz harmonics, which is denoted as the locking rejection region. The measurement demonstrates the stability of the PLL for low-frequency deviations (below 3 kHz), but a wider unstable region for larger frequency deviations. Note that the frequency response peaks at the natural frequency of 12.5 kHz, which is consistent with the step response measurement. This measurement demonstrates that the PLL will lock if the frequency deviation is below 6 kHz, and the FM frequency is below 20 kHz. This is suitable for our system since the Colpitts oscillator was operated between 495 and 520 kHz (frequency deviation of around 10 kHz), with audio frequencies primarily between 6 Hz and 6 kHz (FM frequencies).

5.3 Phase-Locked Loop (Custom-designed Analog Circuit)

[Soojung Bae]

5.3.1 Phase Detector

The schematics of the XOR gate and low-pass filter are depicted in Figure 21. We used simple Resistance-Transistor Logic (RTL) implemented with 2N7000 NMOS transistors. 2N7000 is selected for its low turn-on/off delay time (10 ns) and adequate threshold voltage of $0.8V < V_{th} < 3V$ (Onsemi, 2017). The output of the XOR circuit goes through a low-pass filter with $f_{-3dB} = 19.5\text{kHz}$ which translates the average positive duty cycle of XOR output. Assuming two input signals are at the same frequency, the low-pass filtered output level becomes linear to their phase difference.

The R_1 resistance value decides the circuit's power consumption and transition speed. As shown in Figure 22, we built a simple RTL inverter with 2N7000 (with a drain connec-

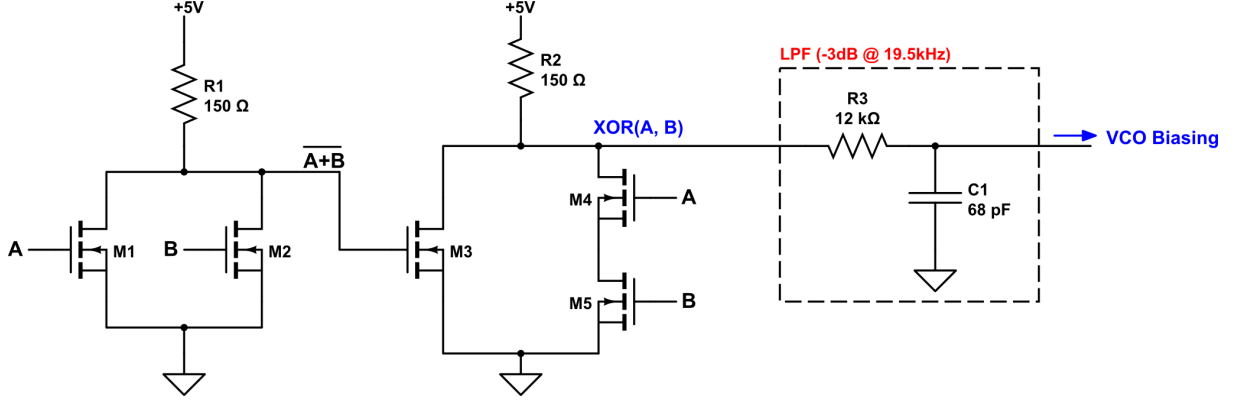


Figure 21: **Phase Detector Circuit.** Left: Resistance-Transistor Logic for XOR gate.
Right: Low-Pass Filter with -3dB frequency = 500kHz.

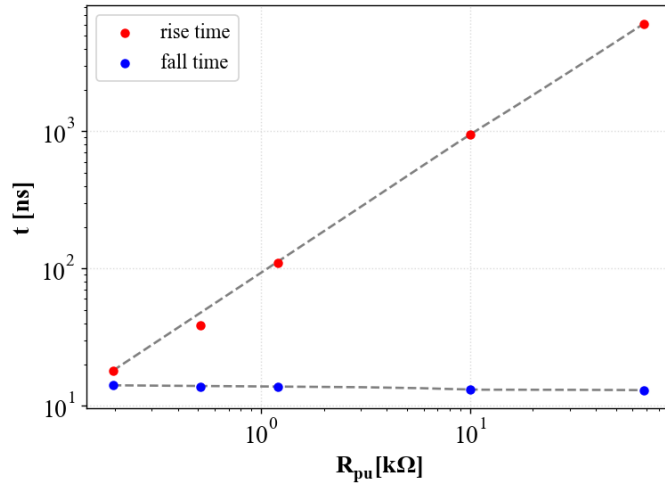


Figure 22: **RTL Inverter Speed vs. Resistance.** Rise and fall time defined as the time required for transitioning between 30% and 70% of the voltage range.

ted to a pull-up resistor R_{pu}) and measured the response time. While fall time is relatively independent of the resistor, rise time is proportional to the resistance value. We chose $R_1 = R_2 = 150\Omega$ such that both rise and fall time are set as approximately 15ns.

Finally, we formed the phase-locking feedback loop by connecting the phase detector output to reverse bias the voltage-controlled oscillator. When the PLL successfully locks to the input signal, the phase detector supplies a constant reverse biasing to VCO with AC ripples, thereby locking not only the phase but also the VCO frequency to the input.

5.3.2 Custom PLL Performance

Figure 23 shows the successful phase-locking results of the PLL. XOR gate produces periodic output locked at the input frequency, thereby ensuring the demodulated signal stays at a constant DC level with ripples. With a 500kHz input signal, the demodulated output had a 2.95V DC offset with 0.3V peak-to-peak ripple voltage.

Figure 24 shows the relationship between the output voltage swing of PLL and the input frequency deviation (i.e., deviation of carrier frequency f_c during modulation). A larger deviation in carrier frequency corresponds to a larger voltage swing driving the

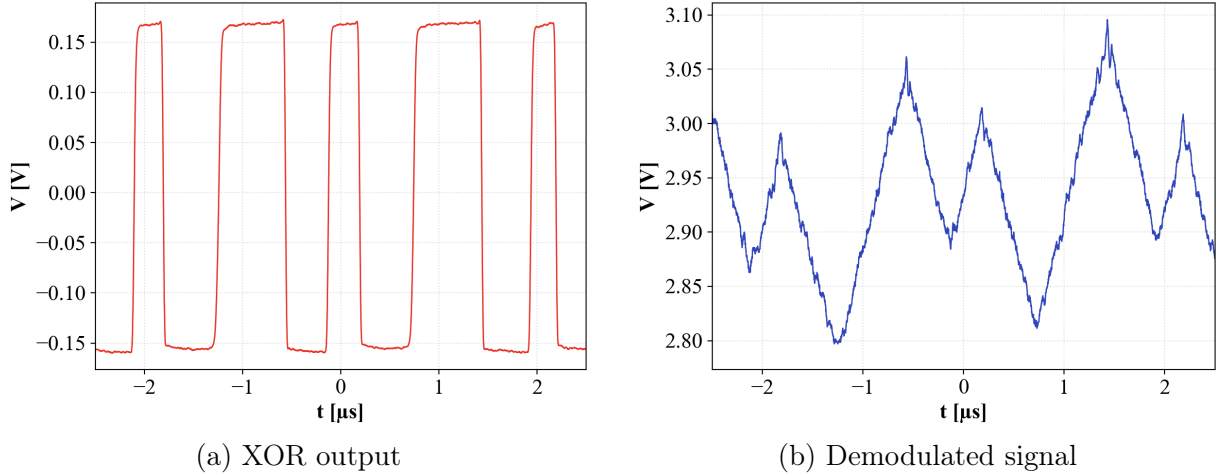


Figure 23: **Phase-locking Functionality Measurement.** PLL made with discrete components successfully locking the 500kHz input signal. Left: XOR gate output. Right: demodulated output (low-pass filtered XOR) driving the VCO.

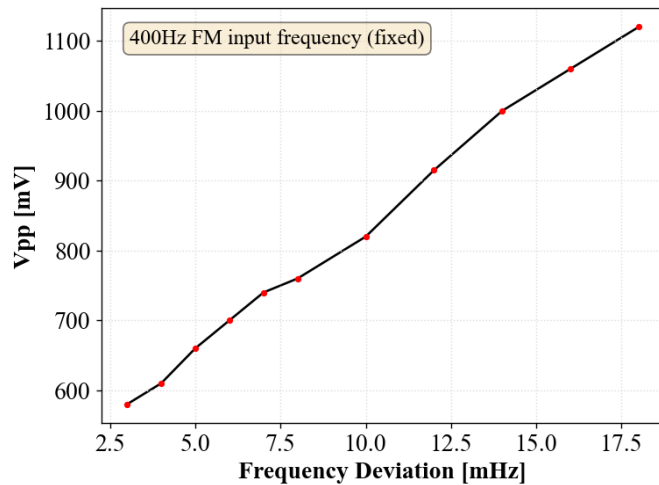
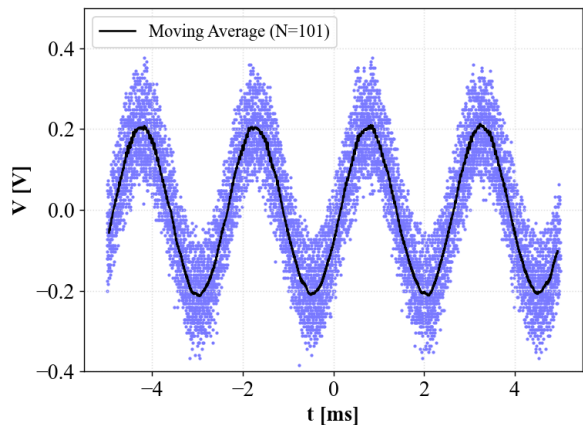


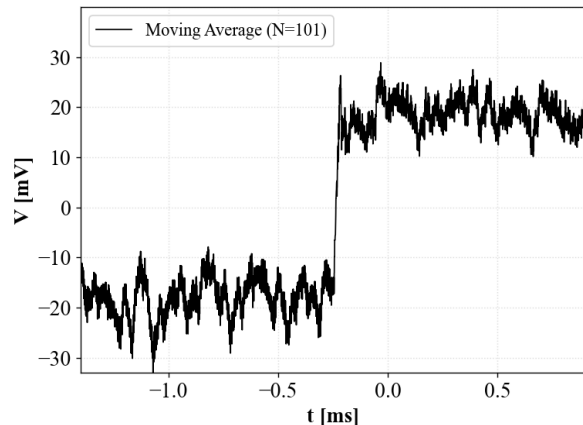
Figure 24: Output V_{pp} with different FM Frequency Deviations. Fixed 400Hz sine input used for modulating the FM signal.

VCO. As expected, using the fixed 400Hz input signal, the output swing has a linear response to the frequency deviation.

The actual demodulation result of the PLL is shown in Figure 25. In Figure 25a, $f_c = 480\text{kHz}$ carrier was modulated with 400Hz sinusoidal input, gradually modulating the carrier frequency by 10kHz deviation. The low-pass filtered result ($f_{-3dB} = 50\text{kHz}$), depicted as a black line, successfully reproduces the 400Hz input signal with 400mVpp swing. In addition, we also verify that the PLL can demodulate the step-wise frequency leaping with stability as shown in Figure 25b. However, due to the smaller frequency response of our VCO compared to the performance of CD4046 IC, we used the Integrated Circuit instead of the custom-designed PLL while demonstrating the audio communication functionality.



(a) Sinusoidal



(b) Square

Figure 25: **Custom-Designed PLL Demodulation Results.** Demodulated output signal from FM 400Hz sine input (left) and from step-function response (right). Low-passed result (moving average) depicted with black lines; filter bandwidth $f_{3dB} = 50\text{kHz}$. FM modulation with 10kHz frequency deviation is used for both graphs.

6. Results

In the end we were able to incorporate all the described components into a functional laser audio communication system. We have successfully transmitted single frequency tones, music and speech through our system. Figure 26 shows the received signal after transmitting a single frequency tone. The yellow signal is the transmitted tone and the pink signal is the received tone. Furthermore, the video demonstration of our fully-functioning system is shown [here](#).

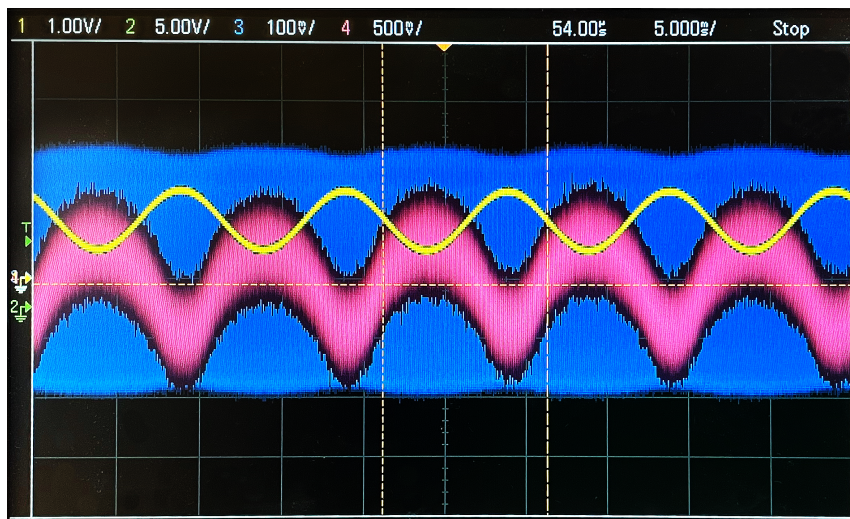


Figure 26: **Full System Modulation/Demodulation:** 100Hz tone received at the end of the signal path. The oscilloscope image shows the input to the transmitter (yellow) and the demodulated output from the CD40406 PLL (pink).

7. Conclusions

For this project we successfully built an audio communication system through a frequency-modulated laser. Our system is divided into three main components: audio, optical, and modulation subsystems. For the audio subsystem, we use operational amplifiers and passive components to bias, amplify, and buffer audio I/O signals. The optical subsystem transmits the frequency-modulated voltage signal through the free-space laser. Finally, we use the Colpitts oscillator to modulate and the phase-locked loop to demodulate the signal. We were also able to build a functional PLL with discrete components.

Some of the more interesting challenges we faced during the project include:

- Driving and receiving the laser at high-frequency without significant attenuation. (the transimpedance amplifier and laser driver)
- Choosing the right component values for the Colpitts oscillator to achieve oscillation at the desired frequency.
- Building the comparator that outputs a 0-6V voltage swing at 500kHz. Several configurations, including the BJT Schmitt Trigger and the cascode amplifiers were tested, but they mainly suffered from low input impedance draining large current during transitions.

In the end, we successfully demonstrated the real-time audio communication through laser fully in the analog domain. Future research to improve the modulation subsystem could explore building a voltage-controlled oscillator with higher linearity in voltage to frequency response, and a high-performance comparator which operates at 500kHz without a significant current drain on the input.

Acknowledgments

We acknowledge our instructor Michael Coln for his insight and guidance, as well as the 6.2040 staff and CIM instructors.

References

- Colpitts, E. H. (1918, February). *Oscillation generator* (No. 1624537). <https://worldwide.espacenet.com/textdoc?DB=EPODOC&IDX=US1624537>
- Hashemi, H. (2015). Transimpedance Amplifiers (TIA): Choosing the Best Amplifier for the Job [<https://www.tij.co.jp/jp/lit/an/snoa942a/snoa942a.pdf>].
- Instruments, T. (2003). CMOS Micropower Phase-Locked Loop [<https://www.ti.com/lit/ds/symlink/cd4046b.pdf>].

- Instruments, T. (2016). LF353 Wide-Bandwidth JFET-Input Dual Operational Amplifier [<https://www.ti.com/lit/ds/symlink/lf353.pdf>].
- Morgan, D. (2003). CD4046B Phase-Locked loop: A Versatile Building Block for Micro-power Digital and Analog Applications [<https://www.ti.com/lit/an/scha002a/scha002a.pdf>].
- Onsemi. (2013). MUR120 Series SWITCHMODE Power Rectifiers [<https://www.onsemi.com/pdf/datasheet/mur120-d.pdf>].
- Onsemi. (2017). 2N7000 / 2N7002 / NDS7002A N-Channel Enhancement Mode Field Effect Transistor [<https://rocelec.widen.net/view/pdf/orqxwkxkq1/ONSM-S-A0003544006-1.pdf>].
- Optoelectronics, L. (2016). Plastic Photodiode Package with Leads pdb-c142 [<https://mm.digikey.com/Volume0/opasdata/d220001/medias/docus/750/PDB-C142.pdf>].
- Semiconductor, R. (2019). 650nm Red Single Mode Laser Diode Datasheet [https://fscdn.rohm.com/en/products/databook/datasheet/ opto/laser_diode/red/rld65nrx200a012-e.pdf].
- Stave, N. J. (2019). Analysis of BJT Colpitts Oscillators - Empirical and Mathematical Methods for Predicting Behavior [Master's Theses (2009 -)]. 554. https://epublications.marquette.edu/theses_open/554].